USING ADAPTIVE SLICING METHOD AND VARIABLE BINDER AMOUNT ALGORITHM IN BINDER JETTING

Hasan Bas [a], Fatih Yapici [a], İbrahim İnanc [b]
[a] Department of Industrial Engineering, Ondokuz Mayis University, Samsun, Turkey
[b] Department of Metallurgy and Materials Engineering, Ondokuz Mayis University, Samsun, Turkey

ABSTRACT

Binder jetting is one of the most important additive manufacturing methods because it is cost-effective, has no thermal stress problems, and has a wide range of different materials. Using binder jetting technology in the industry is becoming more common recently. However, it has disadvantages when compared to traditional manufacturing methods in terms of manufacturing speed. In this study, adaptive slicing was used to increase the manufacturing speed of binder jetting. The real use of adaptive slicing in binder jetting was applied for the first time in this study. In addition, a variable binder amount algorithm has been developed to use adaptive slicing efficiently. Quarter-spherical shaped samples were manufactured using variable binder amount algorithm and adaptive slicing method. Samples were sintered at 1250°C for 2 hours with 10 °C/min heating and cooling ramp. SEM analysis and surface roughness tests were done. According to the results obtained from the analyzes, similar surface quality is achieved by using 38% fewer layers than uniform slicing.

1. Introduction

Additive manufacturing technology was first developed and popularized in the mid-1980s. The first additive manufacturing machine was built and patented by Charles Hull in 1986 [1]. Before Hull's patent, some studies and patent applications have been done [2]. After Hull's patent, many additive manufacturing methods were developed. One of these methods is binder jetting, developed by Sachs et al [3]. Binder jetting is a very important additive manufacturing method and many companies are interested in this technology [4-6]. All kinds of powdered material can be used in binder jetting. Therefore, it has the widest range of materials among all additive manufacturing methods [7-10]. Binder jetting is also one of the most cost-effective additive manufacturing methods and does not require a support structure [11-15]. It is more advantageous to use binder jetting than powder bed fusion methods in terms of thermal stress [16]. Surface roughness and dimensional tolerance are important parameters in manufacturing. There are many studies to investigate surface quality for binder jetting [17-23]. Hartman et al. [24] tried to remove stair-step effect by using the greyscale method. They controlled the saturation by droplet size variation. They used these methods to make sand molds. Rodomsky and Caitlyn [25] also studied the stair-step effect and surface roughness. They manufactured a sample that has surfaces with angles from 5° to 30° at 5° intervals. They observed that the stair step effect is prominent on surfaces between 5° and 20°.

Generally, layer thickness should be reduced in order to improve surface roughness. However, using thin layer thickness increases manufacturing time. Manufacturing time can be reduced by using multiple print heads [10]. Adaptive slicing can be used to increase manufacturing speed. Adaptive slicing was first developed by Dolenc and Makela [26] and is generally used in the fused filament fabrication method.

Persembe et al. [27] have mentioned that adaptive slicing can be used in binder jetting. However, the concept they propose may not be considered to be exactly adaptive slicing. They

manufactured samples with a spherical upper part and a rectangular lower part. The one has 127 μm uniform layer thickness, the second one has 381 μm uniform layer thickness, and the third one has two step layer thickness that layer thickness of the spherical part is 127 μm, and the layer thickness of the rectangular part is 381 μm. But, in order to fully implement adaptive slicing, layer thicknesses must not be constant in the sphere part [27].

In this study, the adaptive slicing method is fully utilized in binder jetting. Quarter-spherical models were used for adaptive slicing. In the sliced models, the layer thicknesses gradually decrease from the bottom region to the top region. In addition, a variable binder amount algorithm was applied in this study. This algorithm is needed because the layer thicknesses are gradually changing. The same amount of binder should not be sent to the layers with different thicknesses. To the best of our knowledge, adaptive slicing has been fully implemented in binder jetting for the first time. Similar surface quality was achieved by using lower number of layers resulting in increasing manufacturing speed.

2. Materials and methods

2.1. Materials and equipment

Commercial alumina powder was used to print the test samples [28]. Miao et al. [29] determined and analyzed the morphology and particle size distribution of the powder. An open-source binder jetting 3D printer [30] was used to investigate adaptive slicing method because commercial binder jetting machines have closed software and hardware, hence it is too hard to implement adaptive slicing. To get better results, some modifications were made to the powder spreader and a rotating roller was added to the 3D printer. A commercial cartridge (HP C6602A) and the black ink of the cartridge were used for printing.

Mitutoyo SJ-400 surface roughness tester used for surface roughness measurement. JEOL JSM-7001F device was used for SEM analysis.

2.2. Adaptive slicing

The open-source Slic3r [31] program was used to adaptively slice the stl. files of the samples. In order to print from the open-source 3D printer, an additional operation is required on the sliced file. Additional open-source software was used to perform this operation [32]. After this operation, the samples can be printed.

2.3. Variable binder amount algorithm

During this study, the variable binder amount algorithm was developed by our research team. Since the layer thicknesses are changing, jetting the same amount of binder on each layer cause problems in adaptive slicing method. In this case, the saturation changes between layers. If the layer thickness is thin and binder amount is high, binder can be spilled out laterally. If the layer thickness is too much and binder amount is too low, binder can’t contact enough to the substrate layers which causes inadequate bonding between layers (Fig. 1). In order to solve this problem, variable binder amount algorithm is developed.

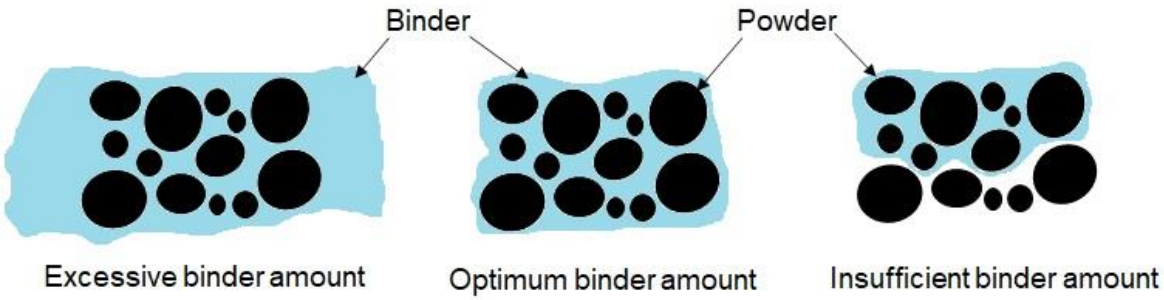

Fig. 1. Relation between binder amount and layer thickness [33]

The steps of the variable binder amount algorithm are shown in Fig. 2. First of all, it is necessary to determine the optimum amount of binder for a specific layer thickness (optimum saturation or calibrated layer thickness and binder amount). In the first step, the Z coordinate is read from the g-code file. In the second step, the Z coordinate value is subtracted from the previous Z coordinate value and the layer thickness is determined. In the third step, the layer thickness is divided by the calibrated layer thickness. In the fourth step, the result obtained in the third step is multiplied by the amount of calibrated binder. By doing so, the required amount of binder is determined and this binder amount is sent from the nozzle.

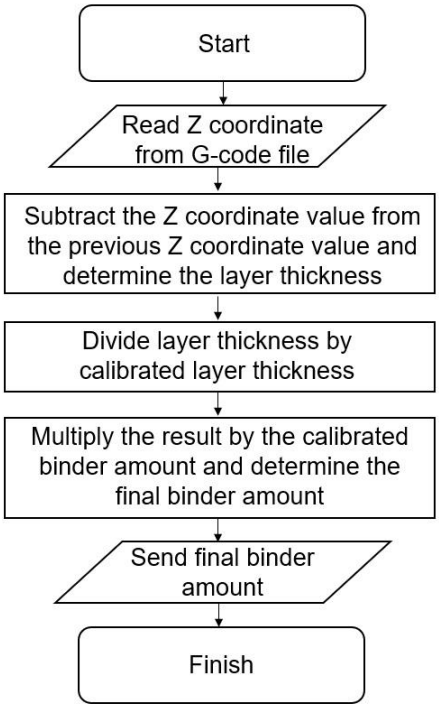

Fig. 2. Variable binder amount algorithm

2.4. CAD models of samples

A quarter-spherical shape was used as a model in this study (Fig. 3). The spherical model was chosen to better understand the effects of adaptive slicing. The radius of the spheres is 9 mm. The lower surface is flatly extended by 2 mm.

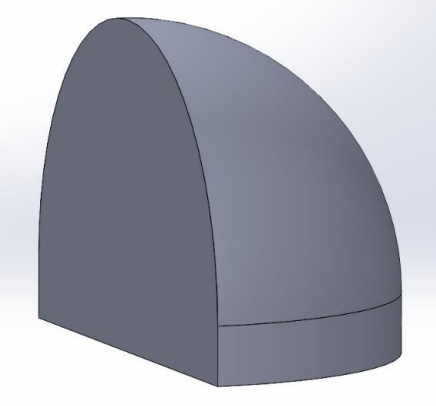

Fig. 3. Quarter-spherical model

2.5. Adaptive sliced samples

Two different adaptive slicing strategies, thick-layered and thin-layered, were preferred. A thick-layered sample was chosen so that the layers can be seen easily with the naked eye.

2.5.1. Thick-layered adaptive sample

The upper limit was chosen as 400 μm in the slicing program. The resulting layer thicknesses are shown in Fig. 4. The total number of layers is 45. The thickness of the first 7 layers is 400 μm, and the thickness of the remaining layers gradually decreases to 150 μm. The three-dimensional view of the sliced thick model (A400-150) is shown in Fig. 5. The layers are clearly visible in the figure.

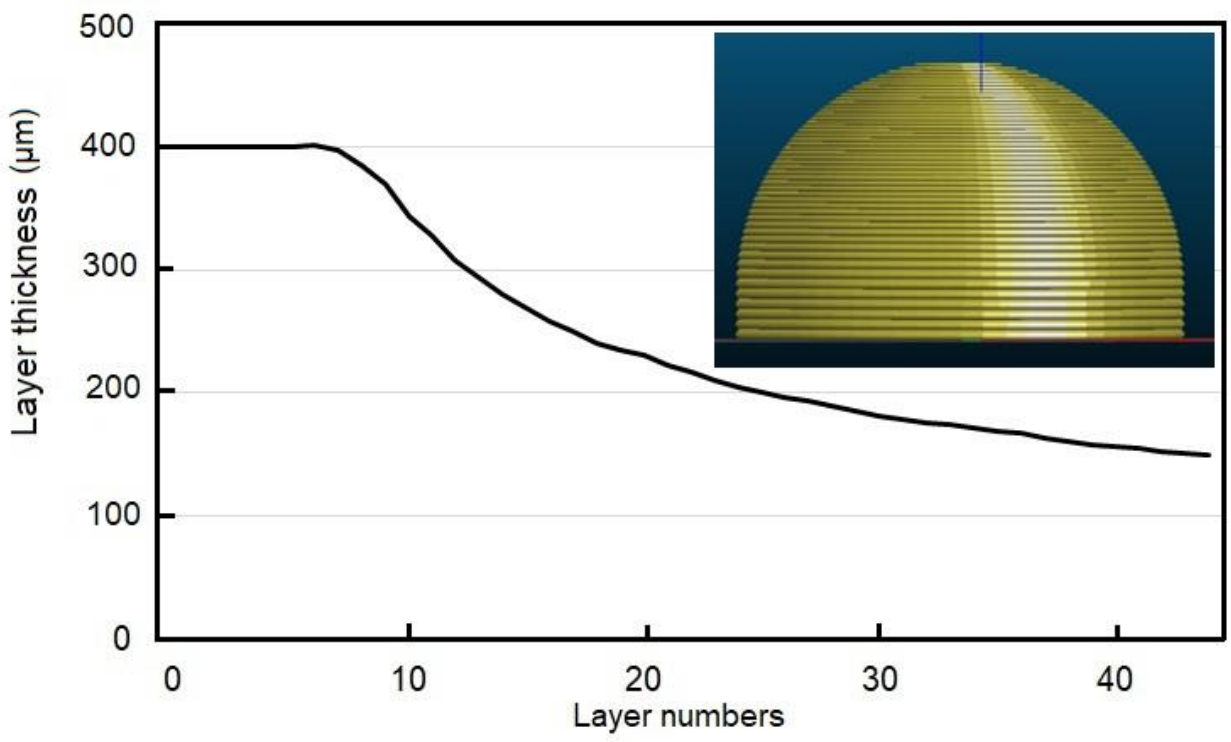

Fig. 4. Layer thickness of the thick model (adaptive)

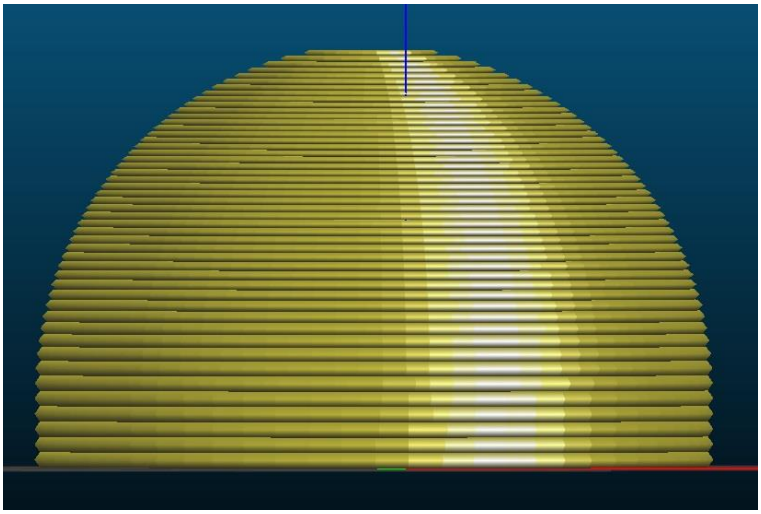

Fig. 5. Thick-layered model (adaptive 0.40-0.15mm)

2.5.2. Thin-layered uniform and adaptive samples

While the sample was sliced adaptively, 60 µm was chosen as the upper limit. The layer thicknesses of the adaptively sliced sample (A60-28) are shown in Fig. 6. There are 242 layers in total. The thickness of the first 59 layers is 60 µm. Later, the thickness gradually decreases to 28 µm. Whereas, layer thicknesses of 28 and 60 µm were used for uniform slicing. A sample of uniform 28 µm (U28) has 392 layers, while a sample of uniform 60 µm (U60) has 183 layers.

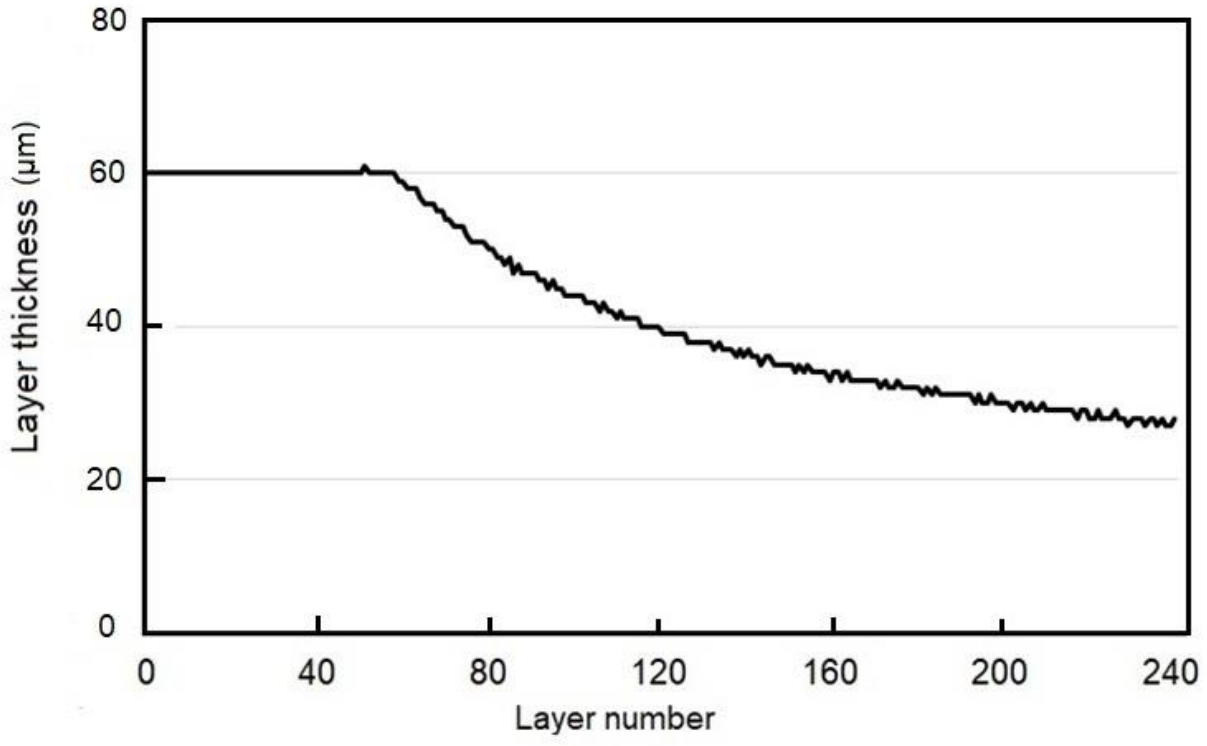

Fig. 6. Layer thickness of the thin layered model (adaptive)

2.6. Printing parameters

The spreader traverse speed was 3 mm/s, the spreader rotation speed was 200 rpm and the printing speed was 40 mm/s. The powder packing rate was measured as 25%. Saturation adjustment is made with a parameter called print density in the used printer. Print density was chosen as 600% and contours were jetted 4 times. According to these parameters, saturation was calculated as 25%.

3. Results and discussions

3.1. Thick layered adaptive sample

A400-150 was manufactured to demonstrate the adaptive layers better (Fig. 7). When looking at this sample, the layers are easily seen. It can be observed that the layer thicknesses decrease from the lower regions of the sample to the upper regions.

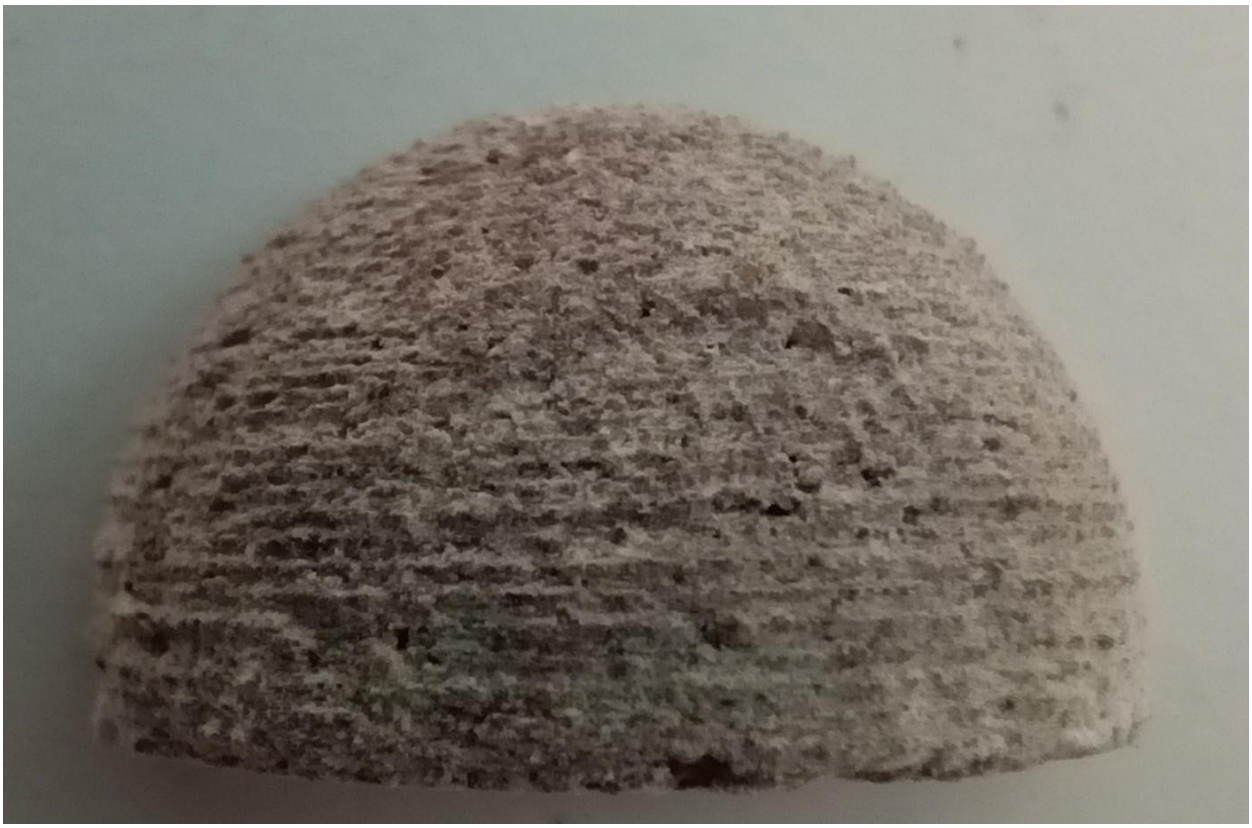

Fig. 7. Thick layered adaptive green part (A400-150)

A400-150 was sintered at 1250° for 2 hours before SEM analysis. SEM images of A400-150 are shown in Fig. 8. Bottom region has a worse surface because of the thick layers (Fig. 8b). It is seen that the surface has improved at the upper region (Fig. 8a).

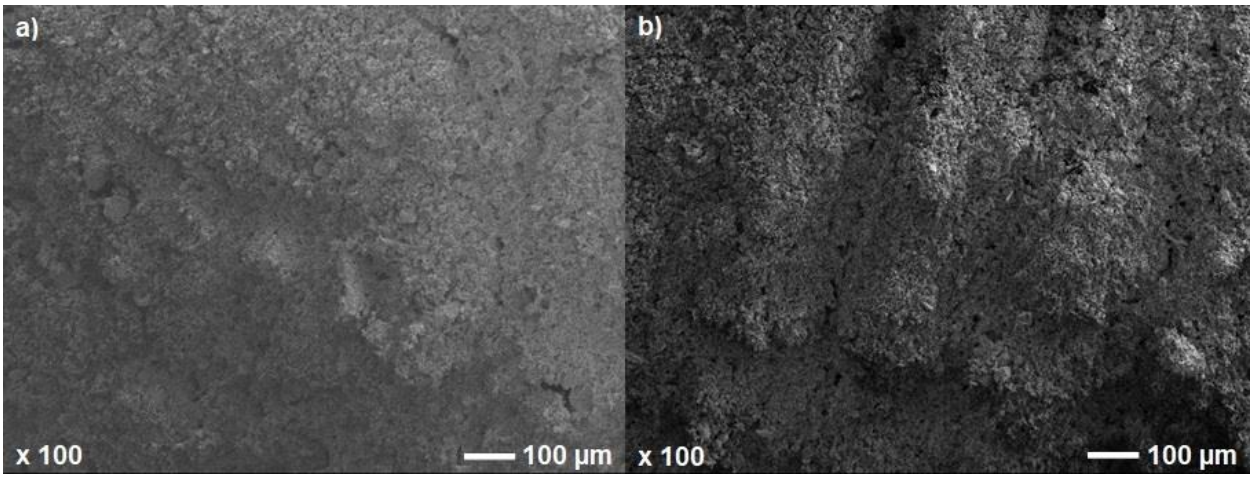

Fig. 8. a) Top region of A400-150, b) bottom region of A400-150

3.2. Thin layered uniform and adaptive samples

Uniform and adaptive samples (green part/unsintered) are shown in Fig. 9. The layers are not visible by naked eye because of the very thin layer thicknesses. The printing time of the U28 took 302 minutes, the U60 took 141 minutes, and the A60-28 took 182 minutes.

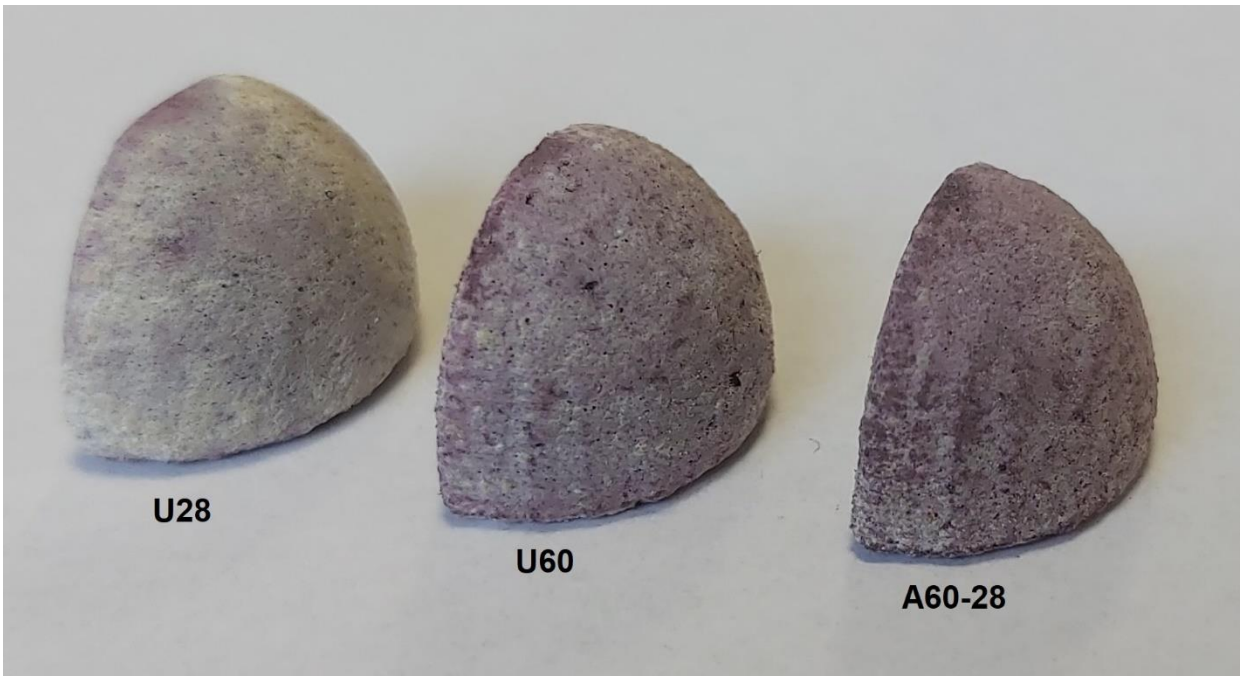

Fig. 9. Thin layered samples (green part)

Quarter spherical samples are sintered at 1250˚C for 2 hours with 10 ˚C/min heating and cooling ramp. SEM images of thin layered samples are shown in Fig. 10. The SEM image of the U28 sample (Fig.10.a) and the SEM images of the A60-28 are similar (Fig. 10.c and Fig. 10.d). But the top surface of the A60-28 has the best quality (Fig.10c). U60 has the worst surface quality (Fig.10b).

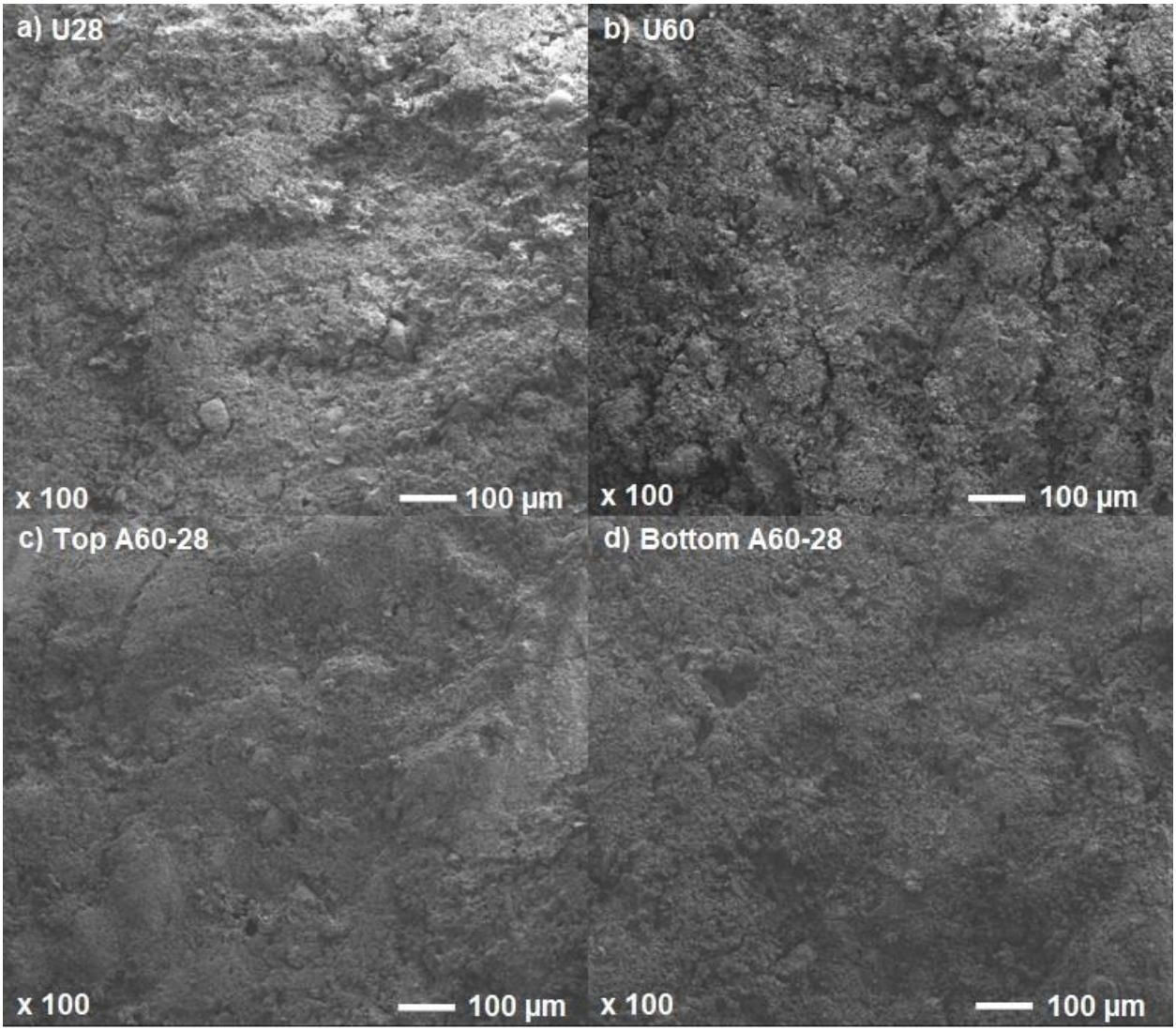

Fig. 10. SEM images of thin layered samples (after sintering). a) U28, b) U60, c) Top region of the A60-28, d) Bottom region of the A60-28.

After sintering, surface roughness tests were made. For each sample, a total of 6 measurements were taken, 3 from the top and bottom regions. A normality test was performed on the obtained data from experiment samples (Tab.1.). According to the results of statistical analysis, it was seen that the data were normally distributed.

Tab.1. Tests of normality.

Sample-region		Shapiro-Wilk		
		Statistic	df	Sig.
Sample	U28	0.876	6	0.251
	U60	0.979	6	0.947
	A60-28	0.925	6	0.541
Region	Bottom Region	0.939	9	0.566
	Top Region	0.946	9	0.651

According to the results of the normality test, it was seen that the data were normally distributed. Since the p-value is less than 0.05, the data shows a normal distribution. The descriptive information about the obtained data is summarized in Tab.2.

Tab.2. Result of the tests.

Sample-region		Mean (μ)	Std. Deviation	Minimum	Maximum	Variance
Sample	U28	10.458	2.051	8.120	14.230	4.206
	U60	12.737	1.559	10.610	14.950	2.431
	A60-28	11.965	0.795	11.070	13.070	0.632
Region	Bottom Region	11.670	1.778	9.620	14.950	3.161
	Top Region	11.770	1.842	8.120	14.230	3.391
Total		11.720	1.757	8.120	14.950	3.086

It has been determined that the measurement values of the surface roughness of samples vary between 8.12 (μm) and 14.95 (μm). It can be said that the decrease in the layer thickness of the sample decreased the value of the surface roughness of samples. The values of surface roughness in the adaptive slicing method were obtained close to the U28. It can be said that the surface roughness value is partially affected by the place where the measurement is taken on the sample surface. The result of variance analysis determined from test samples is given in Tab.3.

Tab.3.The results of variance

Dependent Variable:	Measurement				
Source	Type III Sum of Squares	df	Mean Square	F	Significant Level (p<0.05)
Corrected Model	18.514	5	3.703	1.309	0.324
Intercept	2472.451	1	2472.451	874.040	0.000
Sample	16.113	2	8.056	2.848	0.097
Region	0.045	1	0.045	0.016	0.902
Sample * Region	2.356	2	1.178	0.416	0.669
Error	33.945	12	2.829		
Total	2524.910	18			
Corrected Total	52,459	17			
a. R Squared = 0.353 (Adjusted R Squared =0.083)					

According to the variance analysis, the effects of slicing, measuring region of surface roughness, and interaction of them were not found statically significant at 95% significance level. The comparisons of the means were done by employing a Duncan test to identify which groups were significantly different from other groups, and the results are given in Tab.4.

Tab. 4. The Results of the Duncan Test

Sample	N	Subset	
		Roughness value	Homogenous group (HG)
U28	6	10.458	A
U60	6	11.965	AB
A60-28	6	12.736	B

According to the Duncan test, the surface of the roughness values were determined by changing between 10,458 (µm) and 12,736 (µm). It has been determined that the surface roughness of the samples which are consisting of thin layers (U28) is next close to the surface roughness of the samples made by adaptive slicing (A60-28). It can be said that the surface roughness values of the test samples increase with the increase of the layer thickness. A comparison of surface roughness values is shown in Fig. 11. U28 has the best surface quality. U60 has the worst surface quality. The surface quality of the bottom regions is better in uniform samples. However, the surface quality of the upper region is better in the adaptive sample. Because the layer thickness decreases towards the upper regions. The standard deviation of the measurements was slightly high due to some regional defects on the surface of the samples. This is because the C6602A cartridge has a very low resolution (96 DPI) and black ink is not very adequate as a binder.

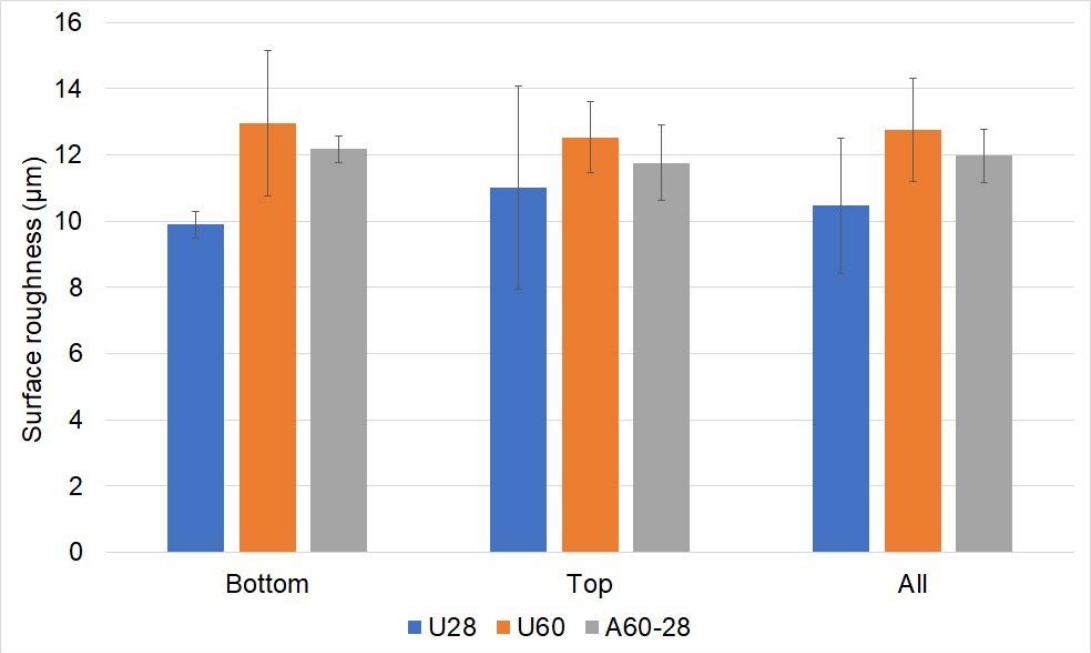

Fig. 11. Comparison of surface roughness

4. Conclusions

Many complex-shaped products are manufactured in the industry. The diversity and complexity of products are increasing day by day with the developing technology. While conventional manufacturing methods are insufficient to meet this need, additive manufacturing methods that have many advantages offer many opportunities. Surface quality and production speed are very important in the manufacturing of very complex shapes. Adaptive slicing can be used to achieve high production rates without reducing surface quality.

The adaptive slicing method has been successfully applied in binder jetting. In addition, a variable binder amount algorithm has been successfully implemented. Products with high surface quality can be manufactured more quickly by using the adaptive slicing method. The adaptive sample (A60-28), U28 and U60 have layers 242, 392 and 183, respectively. The printing time of the U28 took 302 minutes, the U60 took 141 minutes, and the A60-28 took 182 minutes. Although 38% fewer layers are used in A60-28 (adaptive), similar surface roughness is obtained compared with U28, and manufacturing time was reduced by approximately 40%.

It was determined from surface roughness tests that the surface quality of the top region of the sample which was made by using the adaptive slicing method better than the bottom region of the same sample. However, the surface quality of the top and bottom regions of the adaptive sample was similar in the SEM images. The variable binder amount algorithm has a great role in this situation. If this algorithm was not used, more binder would be sent to the thin layers in the upper regions, and therefore the upper regions would have a worse surface. However, if the amount of binder was reduced to compensate for this situation, this time there would be breaks between the layers in the lower regions.

Because of the fact that commercial binder jetting 3D printers have closed software and hardware, open-source printers and software are used in this study. If adaptive slicing is applied to commercial printers, maximum performance can be achieved. As a result, the variable binder amount algorithm and adaptive slicing will play an important role in the binder jetting method in the future.

Credit authorship contribution statement

Hasan Bas: Conceptualization, Writing - original draft, Investigation, Methodology. **Fatih Yapici:** Formal analysis, Writing – review & editing, Supervision, Methodology. **Ibrahim Inanc:** Writing – review & editing, Resources, Methodology, Investigation.

Declaration of Competing Interest

The authors declare that they have no known competing financial interests or personal relationships that could have appeared to influence the work reported in this paper. Thanks are also given to Sampa and Sampa R&D teams for surface roughness measurements.

Acknowledgment

This study was supported by Ondokuz Mayis University with the project of PYO.MUH.1904.21.006.

References

[1] C.W. Hull, Apparatus for production of three-dimensional objects by stereolithography, in: U.S. Patent (Ed.) United States, 1986.
[2] Tessellated, History of Additive Manufacturing. Part I. https://tessellated.eu/en/blog/history-of-additive-manufacturing-part-i/. (Accessed July 27 2022).
[3] E.M. Sachs, J.S. Haggerty, M.J. Cima, P.A. Williams, Three-dimensional printing techniques, in: U.S. Patent (Ed.) United States, 1993.
[4] ExOne, Sand 3D Printers. https://www.exone.com/en-US/3D-printing-systems/sand-3d-printers. (Accessed 20 March 2018).
[5] M. Boström, M. Amnebrink, Sintering Response and Porosity Dependence of Mechanical Properties of Binder Jet Printed MIM-grade 316L, Proceedings - Euro PM2020 Congress and Exhibition, 2020.
[6] voxeljet, VX2000: Highly efficient for sand casting molds up to 2,000 liters. https://www.voxeljet.com/industrial-3d-printer/serial-production/vx2000/. (Accessed 22 August 2022).
[7] B. Utela, D. Storti, R. Anderson, M. Ganter, A review of process development steps for new material systems in three dimensional printing (3DP), Journal of Manufacturing Processes 10(2) (2008) 96-104.

[8] S. Mirzababaei, S. Pasebani, A Review on Binder Jet Additive Manufacturing of 316L Stainless Steel, Journal of Manufacturing and Materials Processing 3(3) (2019) 82.
[9] P.K. Gokuldoss, S. Kolla, J. Eckert, Additive Manufacturing Processes: Selective Laser Melting, Electron Beam Melting and Binder Jetting—Selection Guidelines, Materials 10(6) (2017).
[10] A. Mostafaei, E.L. Stevens, E.T. Hughes, S.D. Biery, C. Hilla, M. Chmielus, Powder bed binder jet printed alloy 625: Densification, microstructure and mechanical properties, Materials & Design 108 (2016) 126-135.
[11] Y. Wang, Y.F. Zhao, Investigation of Sintering Shrinkage in Binder Jetting Additive Manufacturing Process, Procedia Manufacturing 10 (2017) 779-790.
[12] I. Gibson, D. Rosen, B. Stucker, M. Khorasani, Additive Manufacturing Technologies, Springer Nature, Gewerbestrasse 11, 6330 Cham, Switzerland, 2021.
[13] P. Nandwana, A.M. Elliott, D. Siddel, A. Merriman, W.H. Peter, S.S. Babu, Powder bed binder jet 3D printing of Inconel 718: Densification, microstructural evolution and challenges☆, Current Opinion in Solid State and Materials Science 21(4) (2017) 207-218.
[14] A. Mostafaei, S.H.V.R. Neelapu, C. Kisailus, L.M. Nath, T.D.B. Jacobs, M. Chmielus, Characterizing surface finish and fatigue behavior in binder-jet 3D-printed nickel-based superalloy 625, Additive Manufacturing 24 (2018) 200-209.
[15] R. Frykholm, Y. Takeda, B.-G. Andersson, R. CarlstrÖM, Solid State Sintered 3-D Printing Component by Using Inkjet (Binder) Method, Journal of the Japan Society of Powder and Powder Metallurgy 63(7) (2016) 421-426.
[16] A. Mostafaei, E.L. Stevens, J.J. Ference, D.E. Schmidt, M. Chmielus, Binder jet printing of partial denture metal framework from metal powder, Materials Science and Technology Conference and Exhibition 2017, MS and T 2017, 2017, pp. 289-291.
[17] K. Myers, A. Paterson, T. Iizuka, A. Klein, The effect of print speed on surface roughness and density uniformity of parts produced using binder jet 3D printing, Solid Freeform Fabrication 2019: Proceedings of the 30th Annual International Solid Freeform Fabrication Symposium, Austion, Texas, 2019.
[18] H. Miyanaji, N. Momenzadeh, L. Yang, Effect of printing speed on quality of printed parts in Binder Jetting Process, Additive Manufacturing 20 (2018) 1-10.
[19] J.H. Song, H.M. Nur, Defects and prevention in ceramic components fabricated by inkjet printing, Journal of Materials Processing Technology 155-156 (2004) 1286-1292.
[20] S. Huang, C. Ye, H. Zhao, Z. Fan, Additive manufacturing of thin alumina ceramic cores using binder-jetting, Additive Manufacturing 29 (2019) 100802.
[21] I. Rishmawi, M. Salarian, M. Vlasea, Tailoring green and sintered density of pure iron parts using binder jetting additive manufacturing, Additive Manufacturing 24 (2018) 508-520.
[22] H. Zhao, C. Ye, S. Xiong, Z. Fan, L. Zhao, Fabricating an effective calcium zirconate layer over the calcia grains via binder-jet 3D-printing for improving the properties of calcia ceramic cores, Additive Manufacturing 32 (2020) 101025.
[23] K.J. Hodder, R.J. Chalaturnyk, Bridging additive manufacturing and sand casting: Utilizing foundry sand, Additive Manufacturing 28 (2019) 649-660.
[24] C. Hartmann, L. van den Bosch, J. Spiegel, D. Rumschöttel, D. Günther, Removal of Stair-Step Effects in Binder Jetting Additive Manufacturing Using Grayscale and Dithering-Based Droplet Distribution, Materials 15(11) (2022).
[25] C. Rodomsky, B. Conner, Evaluating the surface finish of A356-T6 cast parts from additively manufactured sand molds, Solid Freeform Fabrication 2018: Proceedings of the 29th Annual International Solid Freeform Fabrication Symposium - An Additive Manufacturing Conference, SFF 2018, 2020, pp. 95-116.
[26] A. Dolenc, I. Mäkelä, Slicing procedures for layered manufacturing techniques, Computer-Aided Design 26(2) (1994) 119-126.

[27] E. Persembe, C. Parra-Cabrera, C. Clasen, R. Ameloot, Binder-jetting 3D printer capable of voxel-based control over deposited ink volume, adaptive layer thickness, and selective multi-pass printing, Review of Scientific Instruments 92(12) (2021).
[28] TETHON3D, Tethonite High Alumina Ceramic Powder. https://tethon3d.com/product/tethonite-high-alumina-ceramic-powder/. (Accessed 18 August 2022).
[29] G. Miao, M. Moghadasi, W. Du, Z. Pei, C. Ma, Experimental investigation on the effect of roller traverse and rotation speeds on ceramic binder jetting additive manufacturing, Journal of Manufacturing Processes 79 (2022) 887-894.
[30] YTEC3D, PLAN B. https://ytec3d.com/plan-b/. (Accessed May 14 2019).
[31] Slic3R, Open source 3D printing toolbox. https://slic3r.org/. (Accessed January 2018).
[32] YTEC3D, Software for Plan-B. https://ytec3d.com/plan-b-software/. (Accessed May 14 2019).
[33] A. Mostafaei, A.M. Elliott, J.E. Barnes, F. Li, W. Tan, C.L. Cramer, P. Nandwana, M. Chmielus, Binder jet 3D printing—Process parameters, materials, properties, modeling, and challenges, Progress in Materials Science 119 (2021) 100707.